Study of Optical and Transport Properties of $Cd_{1-x}Zn_xTe$ and $CdSe_xTe_{1-x}$ by Far-IR Reflectance Spectra

Tzuen-Rong Yang,[1] Sheng-Hong Jhang,[1] Yen-Hao Shih,[1] Wan-Ni Cheng,[1]
Fu-Chung Hou,[2] Yu-Chang Yang,[2] P. Becla,[3] Der-Chi Tien,[4] and Zhe-Chuan Feng[2]

[1]*Department of Physics, National Taiwan Normal University, Taipei, Taiwan 116, ROC*
[2]*Graduate Institute of Photonics & Optoelectronics, National Taiwan University, Taipei, Taiwan 106-17, ROC*
[3]*Francis Bitter National Magnet Laboratory, Massachusetts Institute of Technology, Cambridge, Massachusetts 02139*
[4]*Graduate Institute of Mechanical and Electrical Engineering, National Taipei University of Technology, Taipei 10608, Taiwan, ROC*

(Received April 12, 2010)

Far-infrared (FIR) reflectance spectroscopy was employed to study a series of bulk $Cd_{1-x}Zn_xTe$ with varying Zn content (0–100%) and bulk $CdSe_xTe_{1-x}$ with varying Se content (5–35%). The dielectric response function model and least-square fit were used to find the optical and transport parameters. With an increase in the Zn content, the effective mass of $Cd_{1-x}Zn_xTe$ increases slightly, while the carrier concentration increases significantly; however, the mobility and conductivity decrease. With an increase in the Se content, the effective mass of $CdSe_xTe_{1-x}$ decreases slightly, while the mobility, carrier concentration, and conductivity increase significantly.

PACS numbers: 78.20.-e

I. INTRODUCTION

$Cd_{1-x}Zn_xTe$ is a useful substrate material that has the potential to be used in devices, and it is an interesting II-VI compound in its own right. In the 1970s, three groups [1–3] used infrared or Raman spectroscopy to study the transverse-optical (TO) and longitudinal-optical (LO) phonon modes in bulk $Cd_{1-x}Zn_xTe$ at 300 K and 80 K. All three papers reported the two-mode behavior, and they obtained similar plots of the CdTe-like and ZnTe-like TO and LO frequencies versus Zn content. All showed the remarkable result reported by Vodop'yanov *et al.* [2]: unlike every other two-mode system studied at the time, where one mode's TO frequency increases with x while the other mode's TO frequency decreases, in the case of $Cd_{1-x}Zn_xTe$, both frequencies increase with x.

CdTe, CdSe, and their pseudo-binary compounds are very suitable for the fabrication of various optoelectronic devices such as photoconductors, photovoltaic detectors, and photoelectrochemical and solar energy cells; they are also suitable for use as substrates for the growth of quantum wells and epitaxial layers of HgCdTe, HgZnTe, and HgMnTe [4–8]. The II-VI-VI ternary semiconductor $CdSe_xTe_{1-x}$ has the zincblende structure for $x < 0.36$. In this range, its energy bandgap E_g decreases as x increases. Beyond $x = 0.4$, it

exhibits the hexagonal structure and E_g increases and reaches the value for pure CdSe [9]. Several studies on absorption [10] and reflectance [9, 11] have shown that the plot of E_g versus Se content indicates a large bowing effect, with the minimum value of E_g occurring for x values between 0.36 and 0.5. Astonishingly, there is considerable variation among data of different authors. Nahory *et al.* [12] have provided expressions for the bandgaps of quaternary ZnCdSeTe and its boundary ternary alloys, including $CdSe_xTe_{1-x}$, as functions of the composition at 4 K and 300 K. These results have motivated further studies of the bandgap. Earlier investigations of $CdSe_xTe_{1-x}$ with infrared (IR) reflectance [13, 14] and Raman scattering [15] have shown the typical two-mode behavior of the long-wavelength optical phonons. However, Perkowitz *et al.* [16] have reported a third mode, which is attributed to substantial non-random clustering of the anions around the cations. We present here infrared and theoretical studies of four zincblende $CdSe_xTe_{1-x}$ crystals with $x = 0.05, 0.15, 0.25$, and 0.35 and confirm that the third mode previously seen in infrared spectra is a bulk effect. Using a new type of optical spectrometer, we have successfully obtained room temperature spectra of these alloys, which were so far undetectable with the old type of scanning spectrometer.

II. THEORY

From a classical model, the FIR dielectric response function can be expressed as

$$\varepsilon(\omega) = \varepsilon_\infty + \frac{S_j\omega_{Tj}^2}{(\omega_{Tj}^2 - \omega^2 - i\gamma_j\omega)} - \frac{\omega_p^2}{\omega(\frac{\omega+i}{\tau})}$$

where ε_∞ is the high frequency dielectric constant, and ω_{Tj}, S_j, and τ_j are the frequency, strength, and damping constant of the j^{th} TO mode, respectively. The last term in the equation represents the free carrier contribution with a carrier scattering time τ and a plasma frequency of

$$\omega_p = (\frac{4\pi ne^2}{m^*})^{\frac{1}{2}}.$$

Where n is the carrier concentration and m^* is the effective mass. From the dielectric function ε for a system with two oscillators, the strength of TO1 and TO2 can be expressed as

$$S_1\omega_{T1}^2 = \varepsilon_\infty \frac{(\omega_{L1}^2 - \omega_{T1}^2)(\omega_{L2}^2 - \omega_{T1}^2)}{\omega_{T2}^2 - \omega_{T1}^2}$$

$$S_2\omega_{T2}^2 = \varepsilon_\infty \frac{(\omega_{L1}^2 - \omega_{T2}^2)(\omega_{L2}^2 - \omega_{T2}^2)}{\omega_{T1}^2 - \omega_{T2}^2}$$

Where S_j is the oscillator strength of j^{th} mode, ω_{Tj} is the TO frequency of j^{th} mode, and ω_{Lj} is the LO frequency of j^{th} mode. Computer least-square fittings were performed for

all the far infrared reflectivity spectra. The vibration modes and other parameters of the optical and transport modes obtained from these theoretical fits are collected in the section IV Discussion.

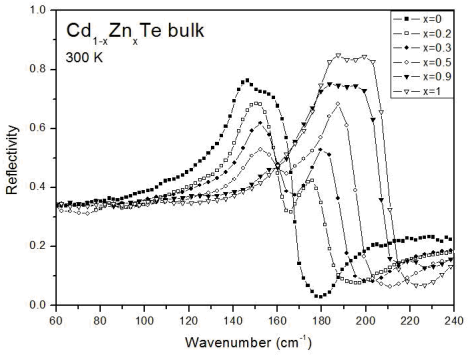

FIG. 1: FTIR reflectivity of bulk $Cd_{1-x}Zn_xTe$ at 300 K with $x = 0, 0.2, 0.3, 0.5, 0.9$, and 1.

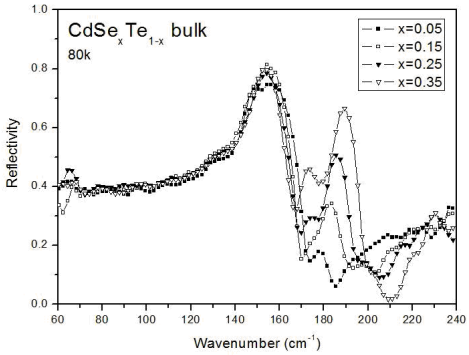

FIG. 2: FTIR reflectivity of bulk $CdSe_xTe_{1-x}$ at 80 K, with $x = 0.05, 0.15, 0.25$, and 0.35.

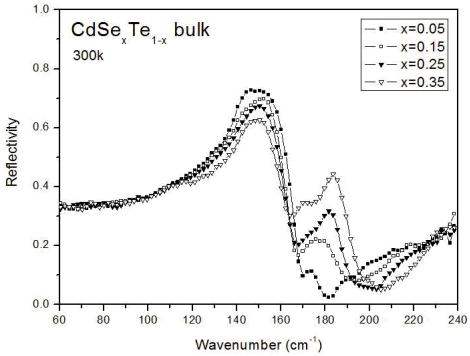

FIG. 3: FTIR reflectivity of bulk $CdSe_xTe_{1-x}$ at 300 K, with $x = 0.05, 0.15, 0.25$, and 0.35.

III. EXPERIMENT

The samples were prepared by the Bridgman technique at Massachusetts Institute of Technology. $CdSe_xTe_{1-x}$ alloys were prepared by reacting the 99.9999% pure elemental constituents at ∼1150 °C in evacuated, sealed quartz tubes. These were regrown by directional solidification at rates of 0.8–1 mm/h in a Bridgman-Stock Barger-type furnace. The resultant boules were cut into slices that were 1–2 mm thick and perpendicular to the growth axis. These were annealed at 650 °C in a Se atmosphere to improve the crystalline perfection. Consequently, they were lapped, polished, and etched in a bromine-methanol solution. The alloy compositions were set by the ratio of constituents before growth, and confirmed by X-ray diffraction and transmission measurements after preparation. These samples were single-crystals with zincblende structure.

The $Cd_{1-x}Zn_xTe$ alloys were made by reacting the 99.9999% pure elemental constituents in evacuated and sealed quartz tubes. The sample x values of 0, 0.2, 0.3, 0.5, 0.9, and 1 were calculated from the mass densities. These precast alloys were regrown by directional solidification in a Bridgman-Stock Barger-type crystal-growth furnace. Regrowth occurred at the rate of 1.2 mm/h in the furnace adiabatic zone with a temperature gradient of about 15 °C/cm. The resulting boules were annealed at 600 °C in a Cd-saturated atmosphere for about 5 d. Their surfaces were prepared by lapping, mechanical polish, and etching in bromine-methanol solution.

Fourier transform infrared (FTIR) reflectivity measurements were made using facilities at National Taiwan Normal University, described elsewhere. A DTGS detector, for good signal-to-noise ratios between 40 and 240 cm^{-1} with resolution of 0.1 cm^{-1} were obtained with a Bruker IFS66 infrared spectrometer. Data were taken at near-normal incidence and at sample temperatures of 300 and 80 K. The incident angle was about 9°, a negligible deviation from normal incidence. The reflection coefficient was measured by rationing the intensity of the light reflected form the sample against that reflected form a reference mirror made of coin silver with about 99% reflectance. In FIGS. 1, 2, and 3, the FTIR reflectivity spectra of the six $Cd_{1-x}Zn_xTe$ samples at 300 K and the four $CdSe_xTe_{l-x}$ samples at 80 K and 300 K are displayed.

In FIGS. 4, 5, and 6, the FTIR reflection spectra of $Cd_{1-x}Zn_xTe$ with x value from 0 to 1, measured at 300 K, and $CdSe_xTe_{1-x}$ with x from 0.05 to 0.35, measured at 80 K and 300 K are shown. For mixed crystals, there are two x-dependent transverse modes, denoted as TO_1 and TO_2, with oscillator strengths S_1 and S_2, as shown in Tables I, II, and III, respectively. In FIG. 4, the vibration mode of $Cd_{1-x}Zn_xTe$ occurring in 141.7 cm^{-1} for $x = 0$ at 300 K is referred to as the CdTe-like mode (TO_1). Also assigned is the ZnTe-like mode (TO_2) at 182 cm^{-1} for $x = 1$ at 300 K. We observed that the CdTe-like TO mode is around 141–153 cm^{-1} for different Zn content at 300 K, and the ZnTe-like TO vibration mode is around 170-182 cm^{-1}. The CdTe-like and ZnTe-like TO modes have a blue-shift with increasing Zn content.

The vibration mode occurring in 144 cm^{-1}, in FIG. 5, for $x = 0.05$ at 80 K is referred to as the CdTe-like mode (TO_1). We can also assign the CdSe-like mode (TO_2) to 177.5 cm^{-1} for $x = 0.05$ at 80 K. We observed that the CdTe-like TO mode is around 144–150

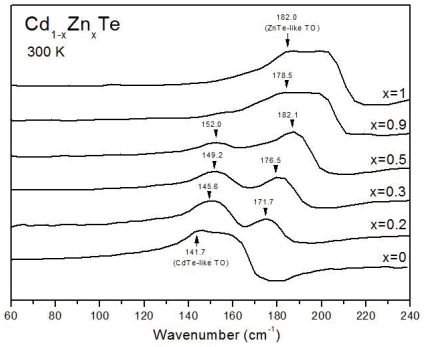

FIG. 4: FIR reflectance spectra of $Cd_{1-x}Zn_xTe$ for Zn content $x = 0$ to 1 at 300 K.

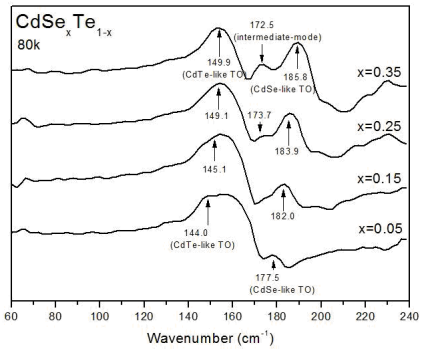

FIG. 5: FIR reflectance spectra of $CdSe_xTe_{1-x}$ for Se content $x = 0.05$ to 0.35 at 80 K.

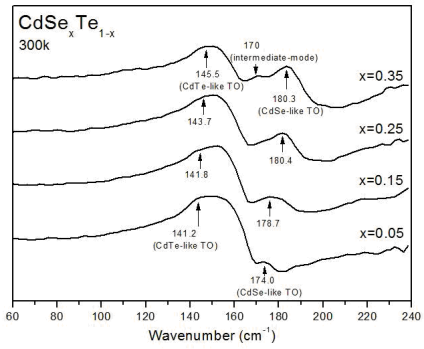

FIG. 6: FIR reflectance spectra of $CdSe_xTe_{1-x}$ for Se content $x = 0.05$ to 0.35 at 300 K.

cm^{-1} for different Se content at 80 K and is around 141–146 cm^{-1} at 300 K. The CdSe-like TO vibration mode is around 177–186 cm^{-1} at 80 K and around 174–181 cm^{-1} at 300 K. The CdTe-like and CdSe-like TO modes have a blue-shift with increasing Se content and a red-shift in between low and room temperature.

IV. DISCUSSION

IV-1. Optical Fits of FIR Reflectance

The LO frequencies were calculated and are shown in FIGS. 7, 8, and 9. The results are similar to the reports of S. Perkowitz [17] and Z. C. Feng [18]. The mode strength versus x plots for bulk $Cd_{1-x}Zn_xTe$ and $CdSe_xTe_{1-x}$ are shown in FIGS. 10, 11, and 12. Tables I, II, and III tabulate the vibration modes and other parameters of the optical modes used on the computed least-square fittings.

With an increase in the Zn content, the CdTe-like TO phonon mode frequency and damping factor increase, but the oscillator strength decreases, whereas the ZnTe-like TO phonon mode frequency and strength increase, and the damping factor decreases with an increase in x. Also, with an increase in the Se content, the CdTe-like TO phonon mode frequency and damping factor increase, but the oscillator strength decreases, while

TABLE I: Optical constants of $Cd_{1-x}Zn_xTe$ at 300 K by dielectric response function fitting.

$Cd_{1-x}Zn_xTe$ 300 K		CdTe-like mode			CdSe-like mode		
x	ε_∞	S_1	$\omega_{TO1}(cm^{-1})$	$\gamma(cm^{-1})$	S_2	$\omega_{TO2}(cm^{-1})$	$\gamma(cm^{-1})$
0	10.44	4.29	141.74	6.83	-	-	-
0.2	8.72	3.22	145.64	9.28	0.47	171.73	10.86
0.3	9.59	3.24	149.19	12.90	0.73	176.52	7.30
0.5	8.56	2.21	152.03	13.72	1.09	182.07	5.60
0.9	11.00	0.02	158.00	0.65	4.29	178.51	6.69
1	9.50	-	-	-	3.39	181.98	3.09

TABLE II: Optical constants of $CdSe_xTe_{1-x}$ at 80 K by dielectric response function fitting.

$CdSe_xTe_{1-x}$ 80 K		CdTe-like mode			CdSe-like mode			intermediate mode		
x	ε_∞	S_1	$\omega_{TO1}(cm^{-1})$	$\gamma(cm^{-1})$	S_2	$\omega_{TO2}(cm^{-1})$	$\gamma(cm^{-1})$	S3	$\omega_{TO3}(cm^{-1})$	$\gamma(cm^{-1})$
0.05	9.68	4.61	144.04	6.01	0.12	177.50	8.53	-	-	-
0.15	10.02	4.52	145.14	6.83	0.33	182.00	11.59	-	-	-
0.25	11.66	4.25	149.07	6.99	0.51	183.88	6.37	0.16	173.70	7.78
0.35	11.70	3.99	149.90	5.92	0.63	185.80	4.78	0.60	172.50	9.00

TABLE III: Optical constants of $CdSe_xTe_{1-x}$ at 300 K by dielectric response function fitting.

$CdSe_xTe_{1-x}$ 300 K		CdTe-like mode			CdSe-like mode			intermediate mode		
x	ε_∞	S_1	$\omega_{TO1}(cm^{-1})$	$\gamma(cm^{-1})$	S_2	$\omega_{TO2}(cm^{-1})$	$\gamma(cm^{-1})$	S3	$\omega_{TO3}(cm^{-1})$	$\gamma(cm^{-1})$
0.05	8.59	3.90	141.18	8.63	0.05	173.99	7.54	-	-	-
0.15	8.74	3.80	141.81	8.03	0.28	178.67	17.16	0.06	174.48	10.11
0.25	8.86	3.74	143.67	11.18	0.33	180.42	11.32	0.10	172.00	10.11
0.35	9.07	3.53	145.46	12.89	0.58	180.32	12.33	0.25	170.00	9.76

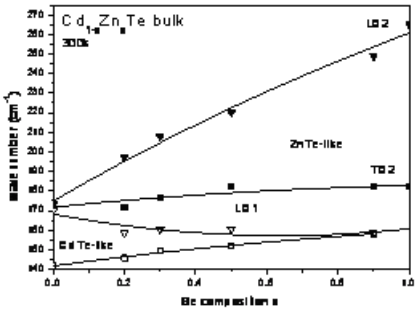

FIG. 7: Optical mode frequency versus x from $Cd_{1-x}Zn_xTe$ bulk at 300 K.

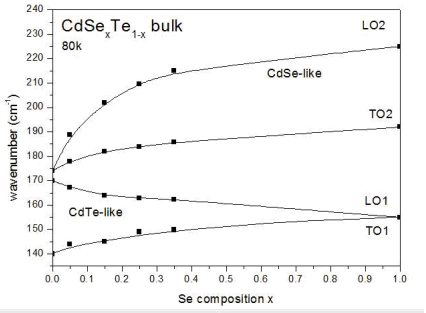

FIG. 8: Optical mode frequency versus x from $CdSe_xTe_{1-x}$ bulk at 80 K.

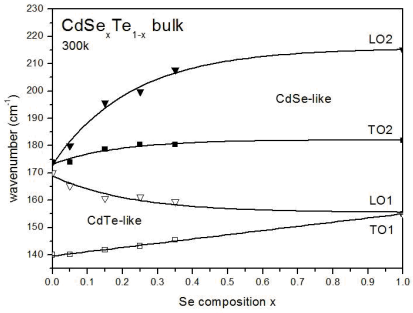

FIG. 9: Optical mode frequency versus x from $CdSe_xTe_{1-x}$ bulk at 300 K.

the CdSe-like TO phonon mode frequency and strength increase, and the damping factor decreases with an increase in x.

IV-2. Transport Fits of FIR Reflectance

The transport properties of these bulks, $Cd_{1-x}Zn_xTe$ and $CdSe_xTe_{1-x}$, can be characterized by also fitting the dielectric response function. The obtained parameter data for the free carrier concentration, mobility, conductivity, and effective mass are listed in Tables

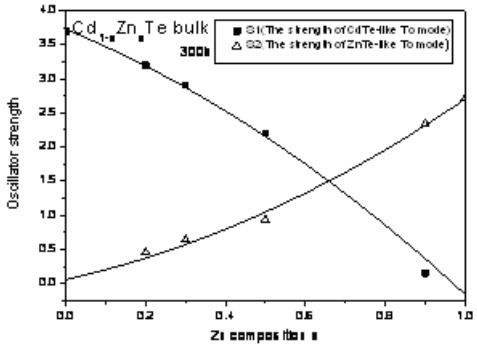

FIG. 10: The mode strength of TO1 and TO2 versus Zn content for $Cd_{1-x}Zn_xTe$ bulk at 300 K.

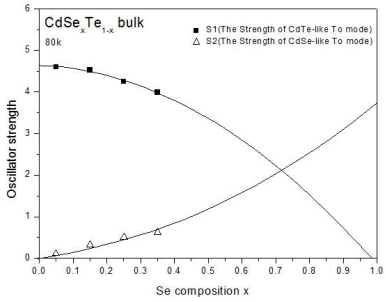

FIG. 11: The mode strength of TO1 and TO2 versus Se content for $CdSe_xTe_{1-x}$ bulk at 80 K.

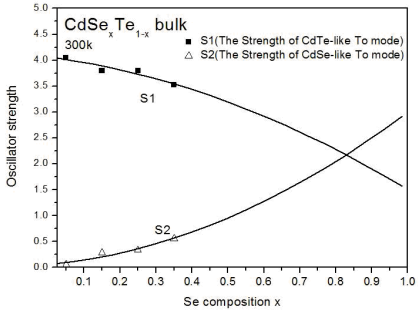

FIG. 12: The mode strength of TO1 and TO2 versus Se content for $CdSe_xTe_{1-x}$ bulk at 300 K.

IV, V, and VI. In Table IV, the effective mass of $Cd_{1-x}Zn_xTe$ increases slightly, whereas the carrier concentration increases greatly with an increase in Zn, but the mobility and conductivity (FIG. 13) decrease with increasing Zn. In Tables V and VI, the effective mass of $CdSe_xTe_{1-x}$ decreases slightly and the mobility, carrier concentration, and conductivity (FIGS. 14 and 15) increase greatly with an increase in Se. An increase in temperature causes the mobility, carrier concentration, and conductivity of $CdSe_xTe_{1-x}$ to increase.

V. CONCLUSIONS

A multitechnique study involving the use of FTIR reflectance was performed on a series of Bridgman-grown bulk $Cd_{1-x}Zn_xTe$ with varying Zn content (0–100%) and bulk $CdSe_xTe_{l-x}$ with the zincblende structure ($x < 0.36$) and varying Se content (5–35%). In FIGS. 1, 2, and 3, it is observed that the phonon modes vary with x. The far infrared reflection spectra showed that the optical quality of these samples is good. Theoretical fits to the FIR reflectivity spectra of all the samples were obtained by using a classical model with the FIR dielectric response function. Composition dependent optical parameters of transverse phonon mode frequency, strength, damping constant have been deduced. Detailed analyses of the FIR reflectance and dielectric function helped improve our understanding of the transport properties of $Cd_{1-x}Zn_xTe$ and $CdSe_xTe_{1-x}$, including the high-frequency-limit dielectric constant, free carrier concentration, mobility, conductivity, and effective mass. The

TABLE IV: Transport properties of $Cd_{1-x}Zn_xTe$ by dielectric response function fitting at 300 K.

$Cd_{1-x}Zn_xTe$ 300 K	Carrier Concentration	Mobility	Effective Mass	Conductivity
x	$10^{16}(cm^{-3})$	(cm2/V s)	m^*/m_e	$10^{-1}(\Omega\ cm)^{-1}$
0	4.34	985.37	0.11	6.84
0.2	3.73	517.82	0.11	3.09
0.3	4.63	483.79	0.11	3.58
0.5	3.63	222.32	0.12	1.29
0.9	3.15	76.31	0.14	0.38
1	8.11	27.07	0.15	0.26

TABLE V: Transport properties of $CdSe_xTe_{1-x}$ by dielectric response function fitting at 80 K.

$CdSe_xTe_{1-x}$ 80 K	Carrier Concentration	Mobility	Effective Mass	Conductivity
x	10^{16} (cm^{-3})	(cm2/V s)	m^*/m_e	$10^{-5}(\Omega\ cm)^{-1}$
0.05	3.27	0.03	0.19655	1.68
0.15	4.14	0.05	0.18995	3.49
0.25	5.88	0.07	0.18375	6.73
0.35	7.21	0.09	0.17795	11.34

TABLE VI: Transport properties of $CdSe_xTe_{1-x}$ by dielectric response function fitting at 300 K.

$CdSe_xTe_{1-x}$ 300 K	Carrier Concentration	Mobility	Effective Mass	Conductivity
x	$10^{17}(cm^{-3})$	(cm2/V s)	m^*/m_e	$10^{-3}(\Omega\ cm)^{-1}$
0.05	5.08	0.29	0.20	2.58
0.15	6.22	0.39	0.19	3.86
0.25	6.48	0.55	0.18	5.67
0.35	6.74	0.78	0.18	9.68

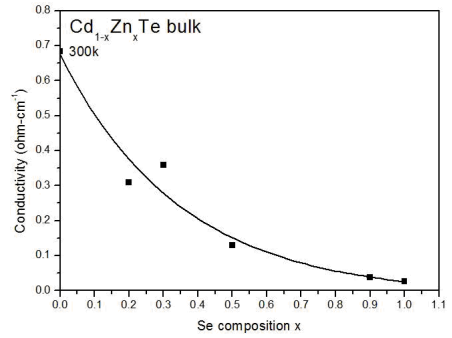

FIG. 13: Conductivity of $Cd_{1-x}Zn_xTe$ dependent on Zn content at 300 K.

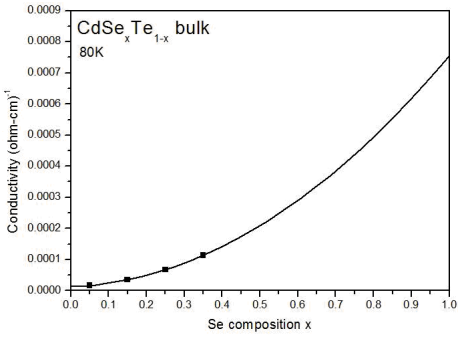

FIG. 14: Conductivity of $CdSe_xTe_{1-x}$ dependent on Se content at 80 K.

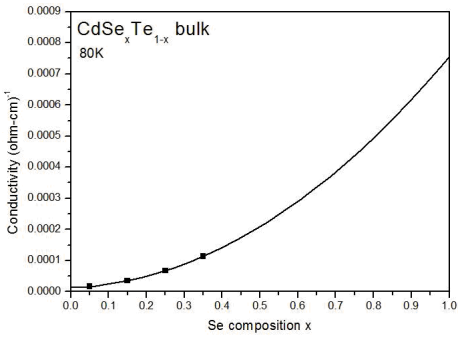

FIG. 15: Conductivity of $CdSe_xTe_{1-x}$ dependent on Se content at 300 K.

fact that these parameters change with x indicates the strong effect of Zn and Se on the transport properties—mobility, carrier concentration, and conductivity; this information is expected to be useful when these materials are used for fabricating devices.

References

[1] H. Narada and S. Narita, J. Phys. Soc. Jpn. **30**, 1628(1970).

[2] L. K. Vodop'yanov, E. A. Vinogradov, A. M. Blinov and V. A. Rukavishnikov, Fiz. Tverd. Tela (leningrand) **14**, 268 (1972)[Sov. Phys.-Solid State **14**,219 (1972)].
[3] E. A. Vinogradov and L. K. Vodopyanov, Fiz. Tverd. Tela (Leninrgrad) **17**, 3161 (1975)[Sov. Phys.-Solid State **17**, 2088 (1976)].
[4] S. M. Babu, T. Rajalakshmi, R. Dhanasekaran and P. Bamasamy, J. Crystal Growth **110**, 423 (1991).
[5] M. Bouroushian, Z. Loizos, N. Spyrellis and G. Maurin, Thin Solid Films **229**, 101(1993).
[6] N. Muthukumarasamy, R. Balasundaraprabhu, S. Jayakumar, M. D. Kannan, Solar Energy Materials & Solar Cells **92**, 851–856 (2008).
[7] Nadir Bouarissa, Physica B **399**, 126–131 (2007).
[8] N. B. Chaure, Shweta Chaure, R. K. Pandey, Electrochimica Acta **54**, 296–304 (2008).
[9] M. S. Brodin, N. I. Vitrikhovskii, A. A. Kipen and I. B. Mizetskaya, Sov. Phys.-Semicond. **6**, 601 (1972).
[10] L. V. Prytkina, V. V. Volkov, A. N. Mentser, A. V. Vanyukov and P. S. Kireev, Sov. Phys.-Semicond. **2**, 509 (1968).
[11] H. Tai, S. Nakashima and S. Hori, Phys. Status Solidi (a) **30**, Kl15 (1975).
[12] M. J. Nahory, S. P. Brasel and M. Tamargo, in: *Semiconductor Interfaces and Microstructures*, Ed. Z. C. Feng, 238 (World Scientific, Singapore, 1992).
[13] M. Gorska and W. Nazarewicz, Phys. Status Solidi (b) **57**, K65 (1973); **65**, 193 (1974).
[14] E. A. Vinogradov, L. K. Vodop'yanov and G. S. Oleinik, Sov. Phys.-Solid State **15**, 322 (1973).
[15] V. G. Plotnichenko, L. V. Golubev and L. K. Vodop'yanov, Sov. Phys.-Solid State **19**, 1582 (1977).
[16] S. Perkowitz, L. S. Kim and P. Becla, Phys. Rev. B **43**, 6598 (1991).
[17] S. Perkowitz, L. S. Kim, Z. C. Feng and P. Becla, Physical Review B **42**, 1455(1990).
[18] Z. C. Feng, P. Becla, L. S. Kim, S. Perkowitz, Y. P. Feng, H. C. Poon, K. P. Williams and G. D. Pitt, Journal of Crystal Growth **138**, 239–243(1994).